Article

Cell Reports

Enclosure of Dendrites by Epidermal Cells Restricts Branching and Permits Coordinated Development of Spatially Overlapping Sensory Neurons

Graphical Abstract

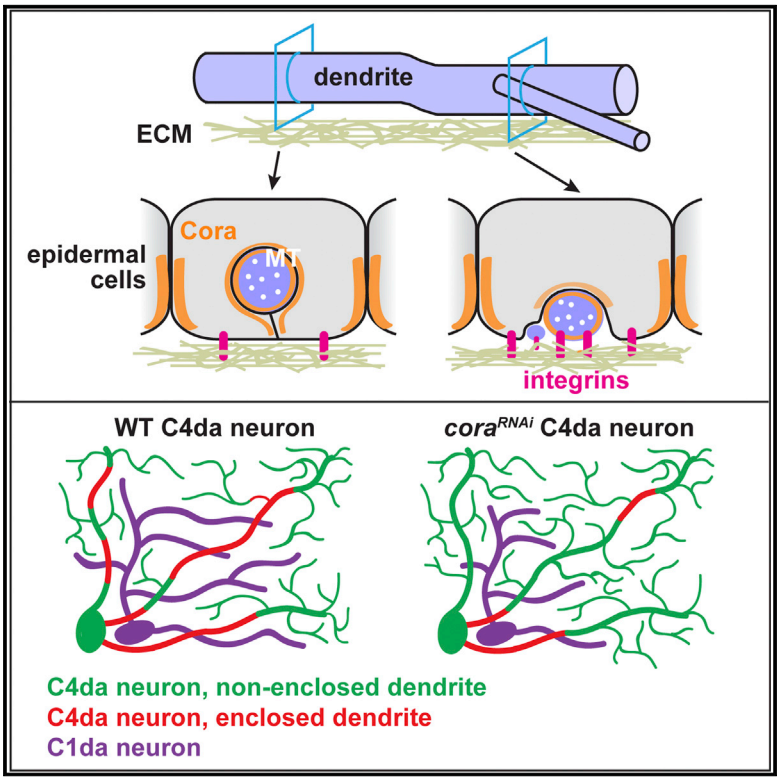

Authors

Conrad M. Tenenbaum, Mala Misra, Rebecca A. Alizzi, Elizabeth R. Gavis

Correspondence

gavis@princeton.edu

In Brief

Tenenbaum et al. show that the membrane-associated protein Coracle locally restricts sensory neuron dendrite branching by promoting enclosure of dendrite segments by epidermal cells. Enclosure counteracts inhibitory interactions between different classes of sensory neurons, suggesting it provides a developmental mechanism for coordinated innervation of shared receptive fields.

Highlights

- Coracle is required for enclosure of C4da neuron dendrites by epidermal cells
- C4da neuron dendrites exhibit local epithelial-like characteristics
- Coracle-mediated enclosure locally restricts dendrite branching
- Enclosure maximizes field coverage among different classes of da neurons

Tenenbaum et al., 2017, Cell Reports *20*, 3043–3056
September 26, 2017
http://dx.doi.org/10.1016/j.celrep.2017.09.001

Cell Reports
Article

Enclosure of Dendrites by Epidermal Cells Restricts Branching and Permits Coordinated Development of Spatially Overlapping Sensory Neurons

Conrad M. Tenenbaum,[1] Mala Misra,[1,2] Rebecca A. Alizzi,[1] and Elizabeth R. Gavis[1,3,*]
[1]Department of Molecular Biology, Princeton University, Princeton, NJ 08544, USA
[2]Present address: Department of Biology, Washington College, Chestertown, MD 21620, USA
[3]Lead Contact
*Correspondence: gavis@princeton.edu
http://dx.doi.org/10.1016/j.celrep.2017.09.001

SUMMARY

Spatial arrangement of different neuron types within a territory is essential to neuronal development and function. How development of different neuron types is coordinated for spatial coexistence is poorly understood. In *Drosophila*, dendrites of four classes of dendritic arborization (C1–C4da) neurons innervate overlapping receptive fields within the larval epidermis. These dendrites are intermittently enclosed by epidermal cells, with different classes exhibiting varying degrees of enclosure. The role of enclosure in neuronal development and its underlying mechanism remain unknown. We show that the membrane-associated protein Coracle acts in C4da neurons and epidermal cells to locally restrict dendrite branching and outgrowth by promoting enclosure. Loss of C4da neuron enclosure results in excessive branching and growth of C4da neuron dendrites and retraction of C1da neuron dendrites due to local inhibitory interactions between neurons. We propose that enclosure of dendrites by epidermal cells is a developmental mechanism for coordinated innervation of shared receptive fields.

INTRODUCTION

Precise spatial arrangement of neuronal receptive fields is essential for the development and function of the nervous system. Tissue territories may be innervated by multiple types of neurons whose spatial coexistence ensures receptivity to their respective sensory or synaptic inputs. As development proceeds, neurons grow or remodel their termini to maintain appropriate field coverage while continuing to share territory with other types of neurons. How neurons of different types coordinate their development to achieve and maintain spatial coexistence in shared receptive fields is poorly understood. In addition, it is unclear what role, if any, non-neuronal support cells play in this developmental process.

The epidermis is innervated by multiple types of sensory neurons that detect and convey information about various external stimuli. The receptive fields of sensory neurons are defined by the morphology of their cutaneous termini, whose development requires intrinsic factors, as well as interactions with epidermal cells, neighboring neurons, and other extracellular cues (Dong et al., 2015). In *Drosophila*, dendrites of four distinct classes (C1–C4) of dendritic arborization (da) neurons with differing sensory modalities occupy largely overlapping fields to innervate the larval epidermis (Grueber et al., 2002).

The *Drosophila* larval epidermis is composed of a single layer of epidermal cells and an underlying extracellular matrix (ECM) comprising the basement membrane. Most da neuron dendrites grow over the ECM near the basal surface of the epidermal cell layer in a largely 2D array. As larval development proceeds, segments of dendrites from the highly branched C4da neurons lose integrin-mediated contact with the ECM and become enclosed within invaginations of the epidermal cell membrane (Jiang et al., 2014), similar to neurites of vertebrate sensory neurons (O'Brien et al., 2012). When integrin-mediated contact of C4da neurons with the ECM is disrupted experimentally, dendrite enclosure is increased and the loss of dendrite-ECM interaction results in aberrant dendrite crossings within and between C4da neuron arbors, possibly by circumventing contact-mediated mechanisms that promote self-avoidance and tiling (Han et al., 2012; Kim et al., 2012). Because dendrite contact with the ECM is critical for self-avoidance and tiling, it is curious that dendrites naturally lose contact with the ECM and become enclosed as development proceeds. This raises the question of whether and what role enclosure plays in normal development.

The molecular mechanisms that govern enclosure have not yet been identified. Interactions between neurons and support cells are often mediated by cell-cell adhesion molecules (McLachlan and Heiman, 2013), and enclosed dendrites of C4da neurons are in sufficient proximity to the membranes of epidermal cells to allow for the formation of adhesive junctions between them. Although several cell-cell adhesion molecules have been shown to be important for C4da neuron development (Hattori et al., 2013; Jiang et al., 2014; Zhang et al., 2014), possible roles of such molecules in mediating dendrite-epidermal adhesion have not yet been characterized.

A subset of proteins typically associated with epithelial septate junctions appears to localize to enclosed dendritic segments (Kim et al., 2012), raising the possibility that these junctional proteins are repurposed by epidermal cells for the development and maintenance of enclosure. Here, we test the hypothesis that the epidermally expressed *Drosophila* protein

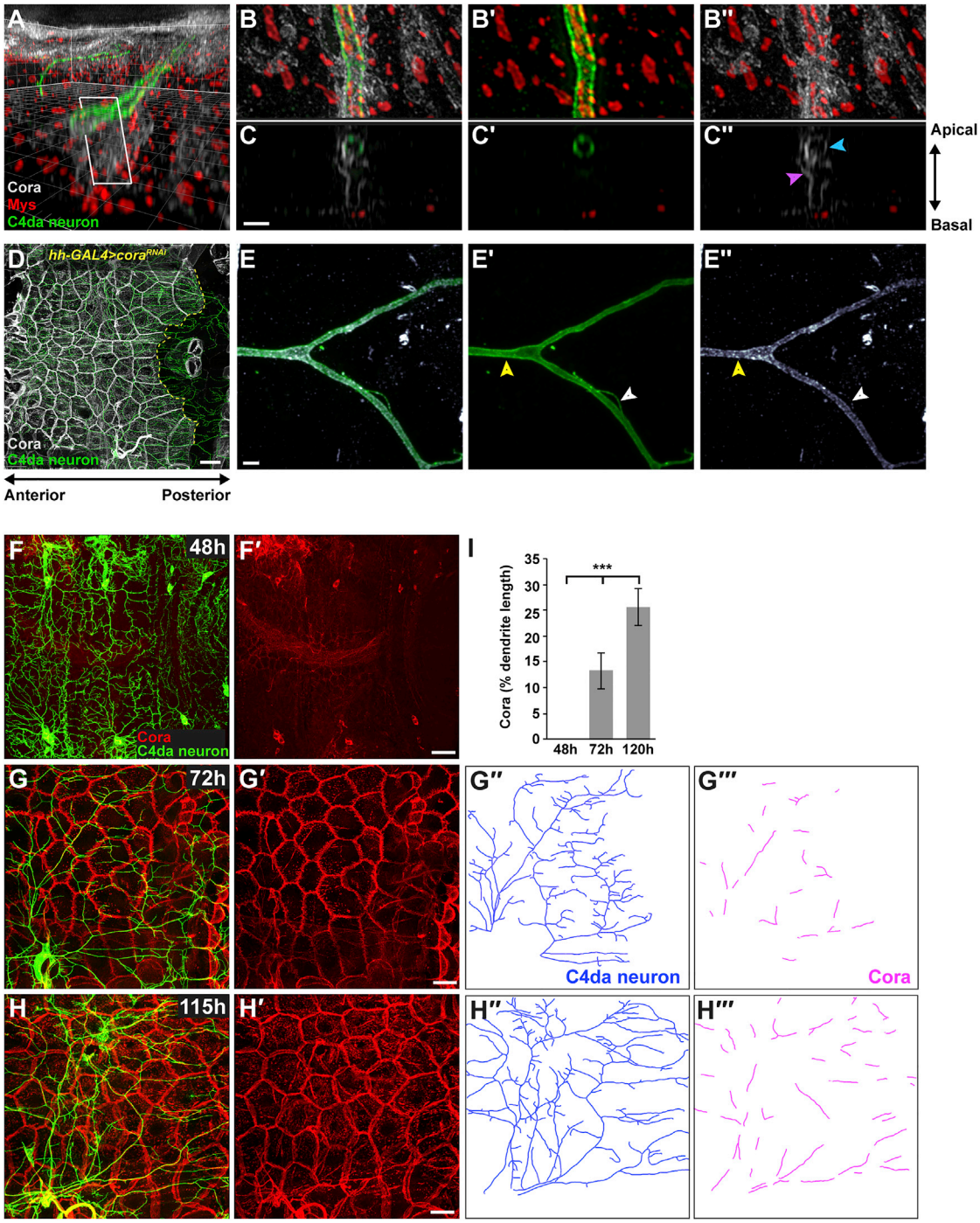

Figure 1. Cora Protein Resides in Both C4da Neurons and Epidermal Cells

(A–C) Immunofluorescence detection of Cora (white) by SIM. C4da neurons (green) were labeled using the *ppk-GAL4* driver to express *UAS-CD4:tdTom*. Anti-Mys immunofluorescence (red) was used to orient the apical-basal axis of the tissue. Merged images for all three detection channels (A–C) and pairwise combinations (B′ and C′) and (B″ and C″). (A) 3D reconstruction of z series projections. (B) A segment of the dendrite in (A) viewed from above. The bottom edges of the images correspond to the position where the neuron is transected by the white box in (A). (C) Cross-sectional planes at the position of the white box in (A). The apical-basal orientation relative to the epidermis and ECM is indicated. The cyan arrowhead indicates Cora at the C4da neuron dendrite membrane; the magenta arrowhead indicates Cora in the epidermis.

(D) Confocal z series projection of a single epidermal segment expressing *UAS-coraRNAi* in the posterior domain (to the right of the dotted yellow line) with *hh-GAL4* and immunostained for Cora (white). C4da neurons were visualized using *ppk-CD4:tdGFP* (green). The anterior-posterior orientation of the larva is indicated.

(legend continued on next page)

4.1 homolog Coracle (Cora) plays such a role. Cora was initially identified as a cytoplasmic component of *Drosophila* septate junctions and subsequently shown to promote epithelial apical-basal polarity (Fehon et al., 1994; Laprise et al., 2009; Ward et al., 1998). Mammalian Cora homologs play a variety of cellular roles, including modulating cell-cell adhesion, cytoskeletal assembly, and β1-integrin surface expression (Baines et al., 2014; Jung and McCarty, 2012). In addition, a missense mutation in the human homolog *EPB41LI* is associated with severe non-syndromic intellectual disability, suggesting a specific role for *EPB41LI* in neuronal function (Hamdan et al., 2011). *Cora* mRNA localizes to dendrites of C4da neurons, and knockdown of *cora* expression results in increased dendrite branching (Misra et al., 2016).

We find that Cora protein is present in closely apposed segments of C4da neuron dendrites and epidermal cells and is required in both cell types for dendrite enclosure. Furthermore, we show that Cora-mediated enclosure occurs preferentially along more proximal dendrites, where it acts to locally restrict branching. In contrast to dynamic terminal dendrites, which continue to grow, retract, and branch throughout larval development, proximal dendritic segments stabilize early, branch infrequently, and contain populations of stabilized microtubules. We propose a model in which proximal dendrites adopt a local epithelial-like profile characterized by microtubule stability and enrichment of some epithelial cell-cell junction proteins, thus allowing them to integrate into the overlying epidermal epithelium.

Our data further reveal a functional role for local epithelial integration of proximal dendrites. We uncover inhibitory interactions between different neuron types and show that local dendritic compartments have differential capacities for coexistence with dendrites of other neurons, highlighting a potential mechanism of neuronal organization. We find that enclosure of C4da neuron dendrites counteracts these inhibitory interactions to permit shared field innervation with C1da neurons. The loss of C4da neuron enclosure and the consequent increase in dendrite branching results in retraction of C1da neuron dendrites, probably via an increase in contact-mediated repulsive interactions. We propose that enclosure of C4da neuron dendrites by epidermal cells represents a coordinated developmental program that locally restricts branching of enclosed dendrites while facilitating morphogenesis of other types of sensory neurons.

RESULTS

Cora Is Expressed in Both C4da Neurons and the Epidermis

We hypothesized that one or more cell-cell adhesion molecules could facilitate interactions between epidermal cells and da neuron dendrites. Cora is one of several septate junction components enriched along enclosed segments of da neuron dendrites (Kim et al., 2012). Previous analysis suggested that Cora enrichment at these segments results, at least partly, from epidermally expressed Cora, but whether Cora is also expressed in da neurons was unclear. To answer this question, we performed anti-Cora immunofluorescence and imaged dendrites and surrounding epidermal cells using structured illumination microscopy (SIM). Myospheroid (Mys), the predominant β subunit (βPS) of the heterodimeric integrin receptor complex (MacKrell et al., 1988; Yee and Hynes, 1993), was visualized using an anti-Mys antibody to orient the apical-basal axis of the epidermal epithelium (Figures 1A–1C). In cross-sections of SIM images, Cora was detected both at the C4da neuron dendrite membrane and in the enclosing epidermal cell, where it was enriched in the region near the dendrite (Figure 1C). To confirm the presence of Cora in dendrites, we knocked down *cora* specifically in epidermal cells using the GAL4/upstream activating sequence (UAS) system. Because pan-epidermal *cora* knockdown was lethal, we used *hh-GAL4* to express *UAS-coraRNAi* in the subset of *hedgehog* (*hh*)-expressing epidermal cells located in the posterior of each larval segment (Tanimoto et al., 2000). *cora* knockdown using *hh-GAL4* almost abolished anti-Cora immunofluorescence in epidermal cells at the posterior of each larval segment (Figure 1D). However, Cora could still be detected in large dendrites that innervate the posterior epidermis (Figure 1E). We conclude that Cora is localized in epidermal cells and in dendrites of C4da neurons, suggesting that it could facilitate dendrite-epidermal interactions.

To ascertain when Cora becomes enriched along da neuron dendrites, we performed anti-Cora immunofluorescence over the course of larval development. At the end of the first larval instar stage (48 hr after egg laying, AEL), when C4da neurons have established their dendritic territories to tile the larval body wall, Cora was detectable at the neuronal cell bodies and epidermal boundaries, but not along the dendrites (Figures 1F and 1I). By the end of the second instar (72 hr AEL), during which C4da neuron arbors grow in concert with the epidermis to maintain tiling, Cora levels were greatly increased at the epidermal cell boundaries, as well as intracellularly, and enrichment of Cora along dendrites was apparent along 13% of the dendrite length (Figures 1G–1G″ and 1I). Cora continued to accumulate during the third larval instar, becoming enriched along 26% of the dendrite length (Figures 1H and 1I).

Cora Is Required to Restrict Dendrite Branching

To determine whether Cora plays a role in dendrite morphogenesis, we examined loss-of-function phenotypes using both mutant alleles and tissue-specific expression of *UAS-coraRNAi* (Figure 2). Null *cora* alleles are lethal during embryonic development due to the requirement for *cora* in dorsal closure

(E) Magnified view of C4da neuron dendrites in the posterior domain of the epidermis shown in (D). Large (yellow arrowhead) and small terminal (white arrowhead) dendrites are indicated.

(F–H) Confocal projections showing anti-Cora immunofluorescence (red) in larvae at 48, 72, and 120 hr AEL. C4da neurons were labeled with CD4:tdGFP (green). Three pairs of dorsal neurons are shown at 48 hr (F and F′); and the dorsal posterior quadrant of the dendritic field is shown at 72 hr (G and G′) and 120 hr (H and H′). The red channel is shown alone in (F′)–(H′). (G″, G‴, H″, and H‴) Tracings of C4da neuron dendrites (blue) and regions of Cora enrichment (pink). Cora enrichment was not detected at 48 hr.

(I) Quantification of Cora enrichment as a percentage of total dendrite length.

Scale bars, 1 μm (B and C), 50 μm (D), 2 μm (E), and 30 μm (F–H). Grid boxes in (A) represent 2 × 2 μm. Values are mean ± SEM; ***$p < 0.001$, as assessed by Student's t test.

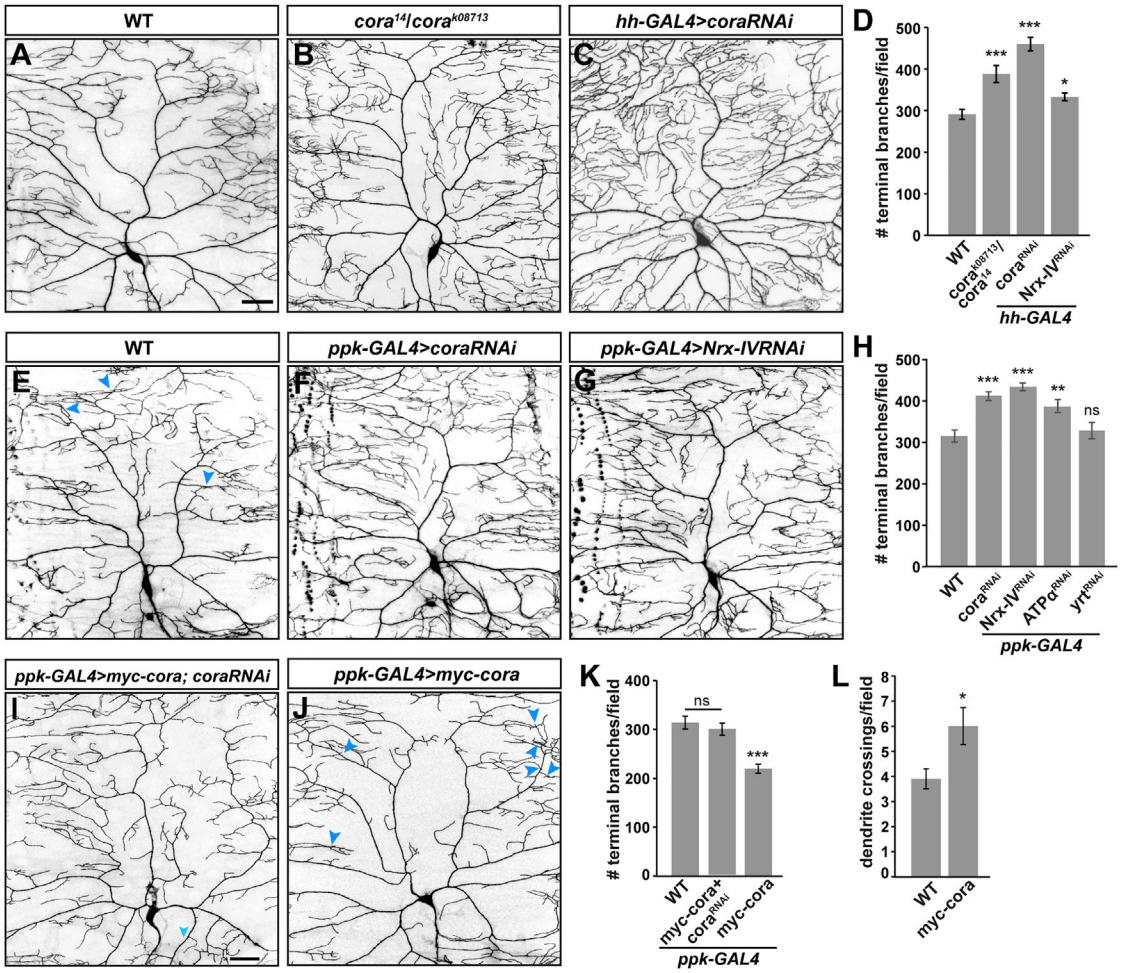

Figure 2. Cora Restricts Dendrite Branching

(A–C) Representative images of C4da neurons labeled using *ppk-CD4:tdGFP* from a wild-type (WT) larva (A), a larva transheterozygous for the hypomorphic *cora*^{14} and *cora*^{k08713} alleles (B), and a larva with epidermal expression of *UAS-coraRNAi* driven by *hh*-GAL (C).

(D) Quantification of the number of terminal branches in the image field for neurons from the indicated genotypes.

(E–G) C4da neurons expressing *UAS-CD4:tdGFP* driven by *ppk-GAL4* either alone (WT) (E) or with *UAS-coraRNAi* (F) or *UAS-Nrx-IVRNAi* (G).

(H) Quantification of the number of terminal branches in the image field for neurons from the indicated genotypes.

(I and J) Neurons expressing *UAS-myc-cora* with *UAS-coraRNAi* (I) or alone (J) using *ppk-GAL4, UAS-CD4:tdGFP*. Although the *myc-cora* transcript is targeted by the RNAi, its overexpression likely partially attenuates the RNAi, leading to a physiological level of *cora* expression.

(K) Quantification of the number of terminal branches.

(L) Quantification of non-contacting dendrite crossings.

All images are confocal z series projections. Blue arrowheads (E and J) indicate non-contacting dendrite crossings. Scale bar, 80 μm. Values are mean ± SEM; NS, not significant; *p < 0.05, ***p < 0.001, as assessed by Student's t test. See also Figure S1.

(Fehon et al., 1994); we therefore generated *cora* mutant larvae using the hypomorphic *cora*^{14} and *cora*^{k08713} alleles (Lamb et al., 1998; Spradling et al., 1999). Third instar larvae that were transheterozygous for these alleles exhibited excess C4da neuron dendrites, suggesting that Cora is required to limit dendrite branching (Figures 2A, 2B, and 2D).

To determine whether this requirement reflects a non-cell autonomous function for Cora in epidermal cells, a cell autonomous function in neurons, or both, we used *hh-GAL4* or the C4da neuron-specific driver *ppk-GAL4*, respectively, to drive expression of *UAS-coraRNAi*. As in *cora* mutants, epidermal knockdown of *cora* resulted in increased dendrite branching in C4da neurons (Figures 2C and 2D). These results were confirmed using a second, independent *UAS-coraRNAi* transgene (data not shown). C4da neuron-specific knockdown of *cora* using either of two *UAS-coraRNAi* transgenes also resulted in increased dendrite branching (Figures 2E, 2F, and 2H) (data not shown). Simultaneous expression of a *UAS-myc-cora* transgene in C4da neurons rescued the RNAi phenotype (Figures 2I and 2K), confirming RNAi specificity.

In *Drosophila* embryos, Cora is required for epithelial polarity during organogenesis. In this context, it interacts with the membrane proteins Neurexin-IV (Nrx-IV) and Na(+)/K(+)-ATPase in a pathway redundant with Yurt (Yrt) to promote basolateral

membrane stability and negatively regulate the apical determinant Crumbs (Laprise et al., 2009). To investigate whether other components of the Cora/Yrt group regulate dendrite branching, we performed RNAi directed against *Nrx-IV*, *Atpα* (encoding the α subunit of Na^+/K^+-ATPase), and *yrt* in C4da neurons. Neuronal knockdown of *Nrx-IV* and *Atpα* produced an overbranching defect resembling that of *cora* RNAi, whereas knockdown of *yrt* did not affect branch number (Figures 2G and 2H). Epidermal knockdown of *Nrx-IV* likewise resulted in increased dendrite branching (Figure 2D). Epidermal knockdown of *Atpα* was lethal even when limited to the posterior region of the segment, precluding our ability to analyze the effect on C4da neurons. Thus, Cora and its transmembrane binding partner Nrx-IV are required in both neurons and epidermis to restrict dendrite branching of C4da neurons. Furthermore, whereas Cora, Nrx-IV, and Na^+/K^+-ATPase may work together in dendrite morphogenesis, as they do in epithelial polarity, the Yrt pathway may not function in this neuronal context.

To determine whether Cora regulates dendrite morphogenesis in other classes of da neurons, we targeted *cora* RNAi to C1da and C3da neurons. In contrast to C4da neurons, knockdown of *cora* did not alter the number of branches or total dendrite length in C1da neurons (Figures S1A–S1D). Similarly, *cora* knockdown in C3da neurons did not significantly alter the density of C3da dendritic spikes (Figures S1E–S1G). We cannot, however, rule out the possibility of insufficient RNAi knockdown in these neurons due to the timing or strength of the respective GAL4 drivers.

Cora Is Required for Dendrite Enclosure

In contrast to loss of *cora*, *cora* overexpression in C4da neurons using *UAS-myc-cora* caused loss of dendritic branches (Figures 2J and 2K). We found that these neurons also exhibited an increase in the number of dendrite crossing events (Figures 2J and 2L). Such a defect, arising from non-contacting dendrite crossings, has been previously associated with increased dendrite enclosure (Han et al., 2012; Kim et al., 2012). We therefore hypothesized that, in addition to its role in restricting dendrite branching, Cora might play a role in promoting dendrite enclosure.

To directly test whether Cora is required for dendrite enclosure, we used an immunofluorescence assay that distinguishes enclosed from non-enclosed dendrite segments (Kim et al., 2012). Binding of anti-horseradish peroxidase (HRP) antibody to neuronal cell surface antigens detects both enclosed and non-enclosed dendrites after tissue permeabilization. Without permeabilization, non-enclosed dendrites are preferentially labeled because they are more accessible than enclosed dendrites. Using this method, we observed that 22% (by length) of wild-type C4da neuron dendrites in third instar larvae were enclosed by epidermal cells (Figures 3A and 3D). This degree of enclosure is comparable to what has been observed using other methods for assaying enclosure (Jiang et al., 2014), and we obtained similar results using the septate junction protein Discs-large (Dlg) to mark enclosed dendrites (Figure S2) (Kim et al., 2012). In agreement with previous work (Jiang et al., 2014), we observed that large primary dendrites were enclosed more often than small terminal dendrites (Figures 3A, 3A″, 3C, and 3C′). To objectively differentiate between large and small dendrites, we labeled C4da neurons with anti-Futsch antibody (Figures 3A′ and 3C″). Futsch, a MAP1B homolog, is a neuron-specific marker of stabilized microtubules and is localized to large primary dendrites but is absent from small higher-order dendrites (Roos et al., 2000; Stewart et al., 2012). In this manner, we observed that Futsch(+) dendrites were 47% enclosed, whereas Futsch(−) dendrites were 7% enclosed (Figure 3E).

Knockdown of *cora* in C4da neurons reduced enclosure to 13%, a >40% decrease compared to wild-type (Figures 3B, 3B″, and 3D). This result was verified using a second independent *UAS-coraRNAi* line (data not shown) and by anti-Dlg immunofluorescence (Figure S2). Consistent with Cora's role in restricting branching, total dendrite branch length was increased in $cora^{RNAi}$ neurons (Figure 3F), and this increase was due primarily to an increase in the total length of Futsch(−) dendrites (Figures 3B′ and 3G). We reasoned that if Futsch(−) dendrites are less enclosed than Futsch(+) dendrites, then the reduced enclosure observed in $cora^{RNAi}$ neurons might simply reflect the higher proportion of Futsch(−) dendrites. To eliminate this possibility, we quantified enclosure of Futsch(+) and Futsch(−) dendrites separately and found that enclosure was reduced for both categories compared to wild-type (Figure 3E). Conversely, *cora* overexpression in C4da neurons caused an increase in enclosure (Figure S3). Finally, knockdown of *cora* in epidermal cells using *hh-GAL4* decreased enclosure of dendrites innervating the posterior portion of the segment by >50% (Figures 3H–3J). Altogether, these results indicate that Cora is required in both the neuron and the epidermis for dendrite enclosure by epidermal cells.

Developmental Characterization of Branching and Enclosure Phenotypes

To determine whether the requirements for Cora in restricting branching and promoting enclosure are independent of each other or causally related, we first determined when during larval development the branching and enclosure defects each manifest. Enclosure of C4da neuron dendrites is first apparent at the beginning of the second larval instar and increases over the remainder of larval development (Jiang et al., 2014). Consistent with this, we observed that wild-type C4da neurons were less enclosed at the end of the second instar, 72 hr AEL, than toward the end of the third larval instar, at 115 hr AEL (22% versus 13%) (Figures 4A and 4C; compare with Figures 3A and 3D). Moreover, these values mirror enrichment of Cora along dendrites (13% at 72 hr AEL and 26% at 120 AEL) (Figure 1I). At 72 hr AEL, C4da neurons expressing *UAS-coraRNAi* already exhibited a nearly 50% reduction in enclosure compared to wild-type neurons at the same stage (Figures 4A–4C). As observed at later stages, enclosure was decreased similarly for Futsch(+) and Futsch(−) dendrites (Figure 4D). In contrast to the effect on enclosure, knockdown of *cora* had no effect on the number of dendritic termini or total dendrite length at 72 hr AEL (Figures 4E–4H). Live imaging of wild-type and $cora^{RNAi}$ C4da neurons at 72 and 115 hr AEL indicated that the overbranched phenotype of $cora^{RNAi}$ neurons observed in third instar larvae arises from an increased growth of new or existing dendrites and decreased retraction of dendrites compared to wild-type neurons (Figure S4). Thus, the effect of *cora* knockdown on branching follows

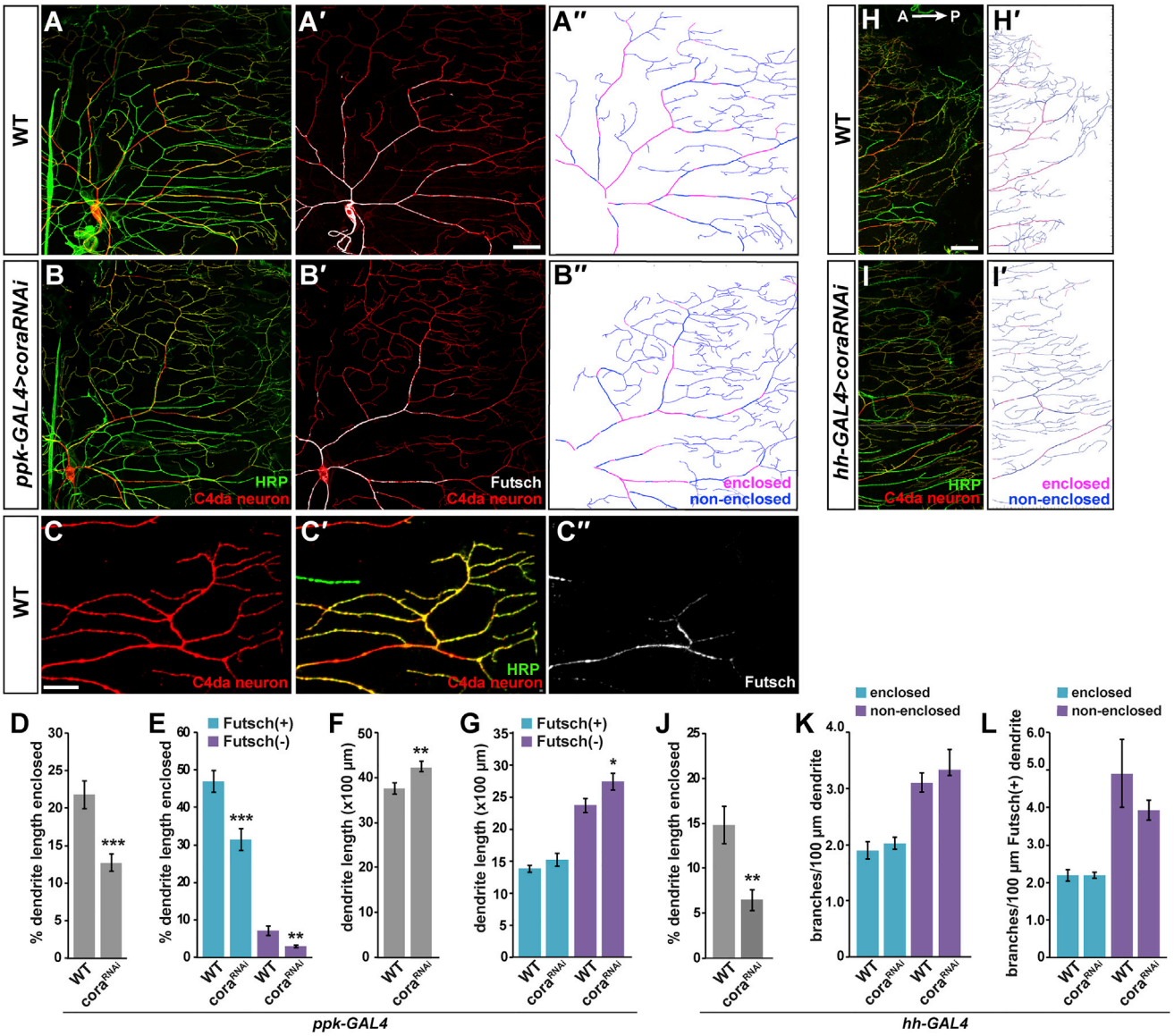

Figure 3. Cora Is Required for Dendrite Enclosure

(A and B) Confocal z series projections showing the dorsal-posterior quadrants of WT (A and A′) and *cora*^{RNAi} (B and B′) C4da neuron dendritic fields. Neurons were labeled with CD4:tdTom (red), and non-enclosed segments of dendrites were identified by anti-HRP immunostaining before permeabilization (green in A and B). Stabilized microtubules were labeled with anti-Futsch antibody (white in A′ and B′). (A″ and B″) Tracings showing enclosed segments (pink) and non-enclosed segments (blue) of the C4da neurons in (A) and (B).

(C) Enlargement of dendrites from a WT C4da neuron labeled as in (A).

(D and E) Quantification of enclosure for all C4da neuron dendrites (D) and for Futsch(+) and Futsch(−) dendrites (E) in the dorsal-posterior quadrant for WT and *ppk-GAL4* > *cora*^{RNAi} larvae.

(F and G) Quantification of total dendrite length (F) and length of Futsch(+) and Futsch(−) dendrites (G).

(H and I) Confocal z series projections showing the posterior field of a C4da neuron from a WT larva (H) or a larva expressing *UAS-coraRNAi* in the posterior epidermis using *hh-GAL4* (I). C4da neurons were labeled using *ppk-CD4:tdGFP* (red). Regions of dendrite enclosure were detected by anti-HRP immunostaining as shown earlier (green). (H′ and I′) Tracings of C4da neuron dendrites in (H) and (I), indicating enclosed (pink) and non-enclosed (blue) segments.

(J) Quantification of dendrite enclosure for WT and *hh-GAL4* > *cora*^{RNAi} larvae.

(K and L) Branch density of WT and *cora*^{RNAi} C4da neurons measured for all dendrites (K) and Futsch(+) dendrites (L).

Scale bars, 30 µm in all panels except 5 µm in (C)–(C″). Values are mean ± SEM; *p < 0.05, **p < 0.01, ***p < 0.001, as assessed by Student's t test. See also Figures S2 and S3.

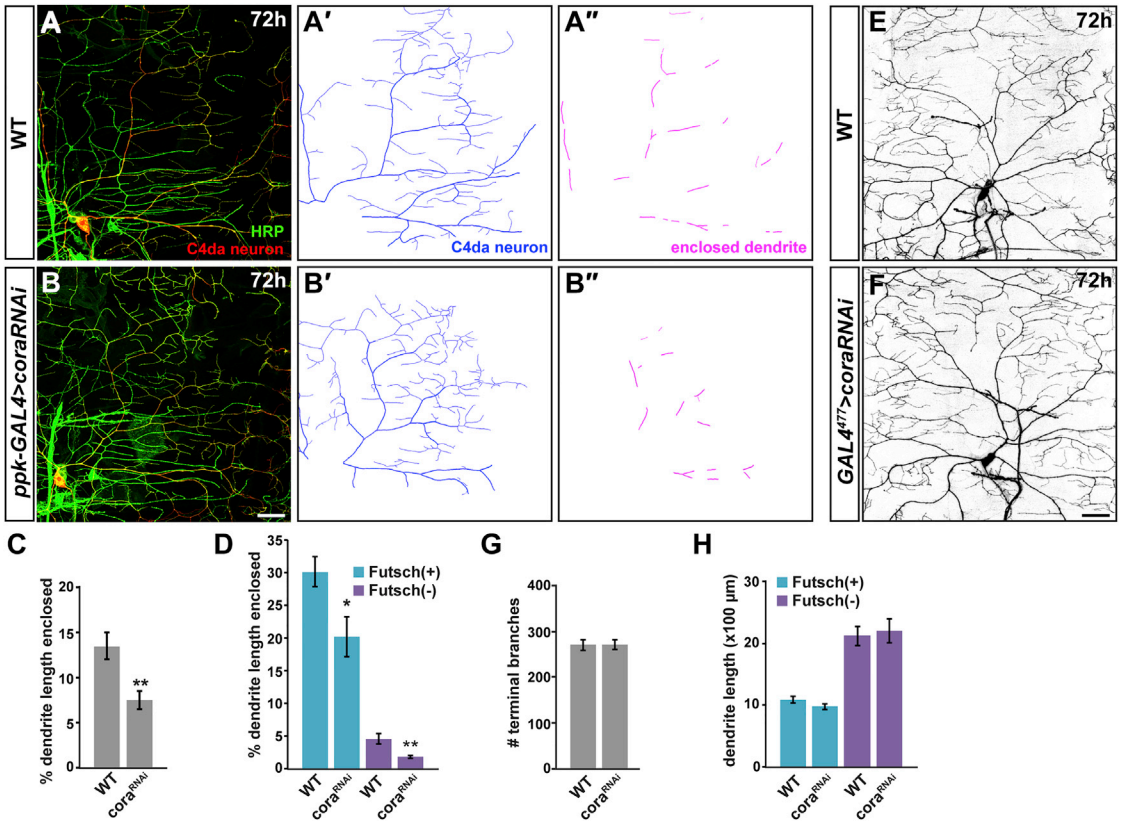

Figure 4. Dendrite Enclosure Precedes Branching Restriction

(A and B) Posterior dendritic fields of WT (A) and *cora*^{RNAi} (B) C4da neurons at 72 hr AEL. Neurons were labeled with CD4:tdTom (red), and regions of dendrite enclosure were detected by anti-HRP immunostaining before permeabilization (green). (A′ and B′) Tracings of C4da neuron dendrites in (A) and (B). (A″ and B′) Enclosed dendrite segments traced from (A) and (B).

(C) Quantification of dendrite enclosure.

(D) Enclosure of Futsch(+) dendrites and Futsch(−) dendrites quantified separately.

(E and F) Representative images of WT (E) and *cora*^{RNAi} (F) C4da neurons at 72 hr AEL labeled with CD4:tdGFP.

(G) Quantification of the number of terminal branches in the image field for neurons from the experiment shown in (E) and (F).

(H) Quantification of dendrite length for Futsch(+) dendrites and Futsch(−) dendrites.

All images are confocal z series projections. Scale bars, 30 μm (A and B) and 40 μm (E and F). Values are mean ± SEM; *p < 0.05, **p < 0.01, as assessed by Student's t test. See also Figure S4.

the effect on enclosure and results from restriction of dendrite retraction and promotion of dendrite outgrowth.

Dendrite Enclosure Locally Restricts Branching

Enclosure of dendrites by epidermal cells is increased when C4da neurons lose integrin-mediated contact with the ECM, as occurs with mutation or knockdown of *mys* or *mew*, which encodes the α1-integrin subunit (αPS1) (Han et al., 2012; Kim et al., 2012). In addition to being more highly enclosed, *mys* mutant C4da neurons have fewer dendritic branches (Kim et al., 2012). Because enclosure of *cora*^{RNAi} neurons was decreased at 72 hr AEL but increased branching was only observed later, we reasoned that Cora might restrict branching by limiting integrin-mediated contact between the dendrites and the ECM. We therefore hypothesized that the excessive branching observed in *cora*^{RNAi} neurons would occur mainly along non-enclosed segments of dendrites, where dendrites contact the ECM. By quantifying the density of branch points along enclosed and non-enclosed dendrites, we found that non-enclosed dendrites were 1.5 times more densely branched than enclosed dendrites in both wild-type and *cora*^{RNAi} neurons (Figure 3K). The increase in branching observed in *cora*^{RNAi} neurons scaled directly with the loss of enclosure. The correlation between enclosure and branching restriction is independent of stable microtubule content (Figure 3L), an important distinction because Futsch(−) dendrites are more highly branched than Futsch(+) dendrites. The decrease in dendrite enclosure in *cora*^{RNAi} C4da neurons can therefore account for the increased branching. Furthermore, these results suggest that Cora may act in opposition to integrins to promote enclosure and restrict branching.

To investigate a functional relationship between Cora and integrins, we used RNAi to knock down *mys* and *cora* simultaneously in C4da neurons and analyzed the effect on both dendrite enclosure and branching. As expected, expression of *UAS-mysRNAi* alone resulted in increased enclosure and decreased branching compared to wild-type neurons (Figures 5A, 5B, 5D,

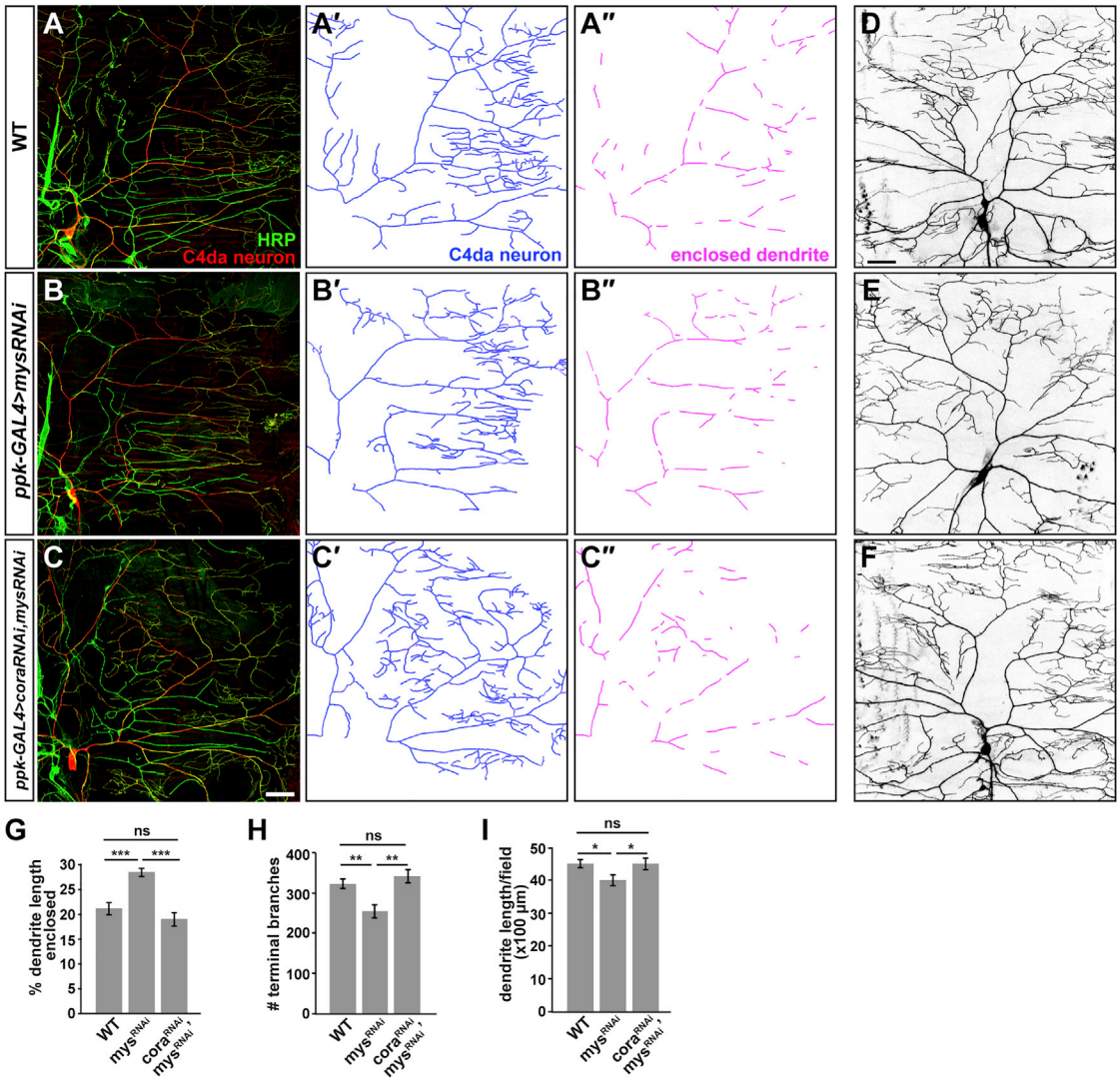

Figure 5. Cora and Mys Control Dendrite Morphogenesis by Regulating Enclosure

(A–C) Dorsal posterior quadrants of the dendritic fields of WT (A), mys^{RNAi} (B), and $cora^{RNAi}$, mys^{RNAi} (C) C4da neurons. Neurons were labeled with CD4:tdTom (red), and non-enclosed dendrite segments were detected by anti-HRP immunostaining before permeabilization. (A′–C′) Tracings of dendrites in (A)–(C). (A″–C″) Enclosed dendrite segments traced from (A) to (C).

(D–F) Representative images of the dendritic fields of WT (D), mys^{RNAi} (E), $cora^{RNAi}$, mys^{RNAi} (F) C4da neurons labeled with CD4:tdGFP.

(G) Quantification of dendrite enclosure for neurons from the experiment shown in (A)–(C).

(H and I) Quantification of the number of terminal branches in the image field (H) and total dendrite length (I) for neurons from the experiment shown in (D)–(F). All images are confocal z series projections. Scale bars, 30 μm (A–C) and 40 μm (D–F). Values are mean ± SEM; *p < 0.05, **p < 0.01, ***p < 0.001, as assessed by Student's t test. See also Figures S5 and S6.

5E, 5G, and 5H). Total dendrite length was also reduced in mys^{RNAi} neurons (Figure 5I). Simultaneous expression of *UAS-mysRNAi* and *UAS-coraRNAi* in C4da neurons suppressed the dendrite enclosure, branching, and length defects (Figures 5C, 5F, and 5G–5I). Conversely, simultaneous overexpression of *mys* and *mew* dramatically increased dendrite branch number and length and reduced dendrite enclosure by more than 3-fold (Figures S5A, S5B, and S5E). Similar to *cora* RNAi, overexpression of *mys* and *mew* resulted in increased prevalence of Futsch(−) dendrites, but the effect on enclosure was independent of stable microtubule content (Figures S5A′, S5B′, S5F, and S5G). Altogether, these data indicate that Cora and Mys play functionally opposing roles in dendrite morphogenesis, likely by regulating the degree of dendrite enclosure.

We also investigated whether the relationship between enclosure and branching observed for C4da neurons extends to other classes of da neurons. Wild-type C1da neurons are only minimally enclosed (Kim et al., 2012) (Figures S6A and S6C). *cora* overexpression in C1da neurons was sufficient to increase enclosure, reduce branching, and reduce dendrite length

(Figures S6B–S6E), suggesting that as in C4da neurons, enclosure of C1da dendrites is associated with reduced branching and branch length. In addition, major dendrites of C3da neurons are partially enclosed, and some regions of Cora enrichment along these dendrites is evident (Kim et al., 2012) (Figures S6F and S6H). Dendrite spikes were nearly absent from enclosed segments of C3da neuron dendrites, suggesting that enclosure may limit outgrowth of these dendritic extensions (Figures S6F and S6I). Expression of *UAS-coraRNAi* in C3da neurons did not significantly reduce dendrite enclosure (data not shown), but overexpression of *mys* and *mew* together reduced enclosure by approximately 30% (Figures S6G and S6H). Compared to wild-type neurons, C3da neurons overexpressing *mys* and *mew* showed a roughly 30% increase in spike density, entirely on non-enclosed dendrites (Figures S6I and S6J). Thus, the density of C3da neuron dendritic spikes scales inversely with the extent of dendrite enclosure. Taken together, these results provide evidence that dendrite enclosure is directly coupled to local branching restriction in da neurons.

Enclosure Facilitates Heterotypic Dendrite Crossings

C4da and C3da neurons share their territory with other, less enclosed da neurons. For example, the dorsal-posterior quadrant of the C4 ddaC neuron shares its dendrite field with the comparatively non-enclosed C1 ddaE neuron (Grueber et al., 2003). We hypothesized that enclosure might separate dendrites of ddaC and ddaE neurons in 3D space to permit heterotypic dendrite crossings within the territory shared by these neurons. In support of this idea, we observed that 55% of crossing events between ddaC neurons and ddaE neurons occurred where the ddaC neuron was enclosed and thus where dendrites of the two neuron types were not contacting each other (Figures 6A and 6D). This number is consistent with previous observations suggesting that heterotypic dendrite crossings preferentially occur where one of the two dendrite segments is enclosed (Kim et al., 2012). Given that only 22% of ddaC neuron dendrite length was enclosed (Figure 3D; expected wild-type value in Figure 6D), the occurrence of crossing events at enclosed segments of ddaC neurons appeared to be non-random. This tendency persisted even when enclosure was reduced by knockdown of *cora* in C4da neurons or by neuronal *mys, mew* overexpression (Figures 6B–6D). Furthermore, *cora* RNAi and *mys, mew* overexpression each resulted in fewer crossings between dendrites of ddaC and ddaE neurons than in wild-type, even though Sholl analysis showed that the prevalence of ddaC neuron dendrites in the field normally innervated by ddaE neurons was increased (Figures 6B, 6B″, 6C, 6C″, 6F, and 6G; also see Figure 7H). That enclosure of C4da neurons facilitates dendrite crossings with C1da neurons suggests a contact-dependent form of recognition between the two neuron types.

We also observed that while C1da neuron dendrites readily crossed Futsch(+) dendrites of C4da neurons, C1da neuron dendrites and Futsch(−) dendrites of C4da neurons appeared to avoid each other, creating a pattern of heteroneuronal dendrite intercalation (Figures 6A′–6A‴, 6B′–6B‴, and 6C′–6C‴). As a result, only 20% of crossing events between ddaC neurons and ddaE neurons occurred where dendrites of the ddaC neuron were Futsch(−) (Figure 6E). This is striking given that Futsch(−) dendrites constituted 65% of the length of C4da neuron dendrites (Figure 6E; expected wild-type value from Figure 3G) and suggests that crossings by C4da neuron preferentially occur where dendrites are Futsch(+). This tendency persisted after neuronal knockdown of *cora* or neuronal *mys, mew* overexpression, even though the length of Futsch(−) C4da neuron dendrites increased (Figures 3G and 6E; Figure S5F). Furthermore, crossings that occur where dendrites are Futsch(−) were more strongly biased toward regions where the dendrite was enclosed than crossings where dendrites were Futsch(+) (Figures 6F and 6G). Altogether, these results suggest that enclosure and possibly microtubule content of C4da neuron dendrites are permissive for crossing of C1da neurons by C4da neurons.

Enclosure Permits Shared Field Innervation by Heterotypic Neurons

We reasoned that shared field innervation between C4da and C1da neurons depends on the ability of their dendrites to cross each other. Because *cora* knockdown in C4da neurons reduced the occurrence of dendrite crossings between the two neuron types, we sought to determine whether and how enclosure of C4da neurons affects C1da neuron morphogenesis. To examine this, we monitored the development of ddaE neurons with respect to ddaC neurons at 72 and 115 hr AEL, the time frame when we observed *cora* RNAi effects on C4da neurons. At 72 hr AEL, ddaE neurons averaged 23 dendrites and an approximately 1,150 μm total dendrite length (Figures 7A, 7F, and 7G). By 115 hr AEL, the total dendrite length increased to 1,400 μm while the dendrite number remained the same (Figures 7C, 7F, and 7G). This period of C1da neuron dendrite elongation coincided with the growth of the C4da neuron arbor, which increased in both total dendrite length and dendrite number (Figures 2D, 3F, and 4G). The number of crossing events between C1da and C4da neuron dendrites increased by approximately 50% from 72 to 115 hr AEL (Figure 7H). When expression of *UAS-coraRNAi* was targeted specifically to C4da neurons, C1da neurons resembled their wild-type counterparts at 72 hr AEL (Figures 7B, 7F, and 7G). By 115 hr AEL, however, dendrite number decreased by 35% relative to wild-type (Figures 7D and 7F), whereas total dendrite length remained unchanged (Figure 7G), indicating that significant dendrite retraction occurred during this period. These results were replicated with *cora* knockdown in C4da neurons by two independent GAL4 drivers (data not shown). Decreasing enclosure by overexpression of *mys* and *mew* in C4da neurons had a similar effect on C1da neurons to *cora* knockdown (Figures 7E–7H). However, increased enclosure of C4da neurons induced by *mys* RNAi did not result in excess branching or growth of C1da neurons (data not shown). Together these data indicate that enclosure of C4da neurons is necessary, but not limiting, for C1da neuron arborization during larval growth. Furthermore, we conclude that enclosure facilitates the simultaneous development of the two neuron types by enabling separation of dendrites along the apical-basal axis of the epidermis and by locally restricting the outgrowth of Futsch(−) C4da dendrites.

C1da neuron arbors also overlap with those of C3da neurons but to a lesser extent than with C4da neurons. To determine

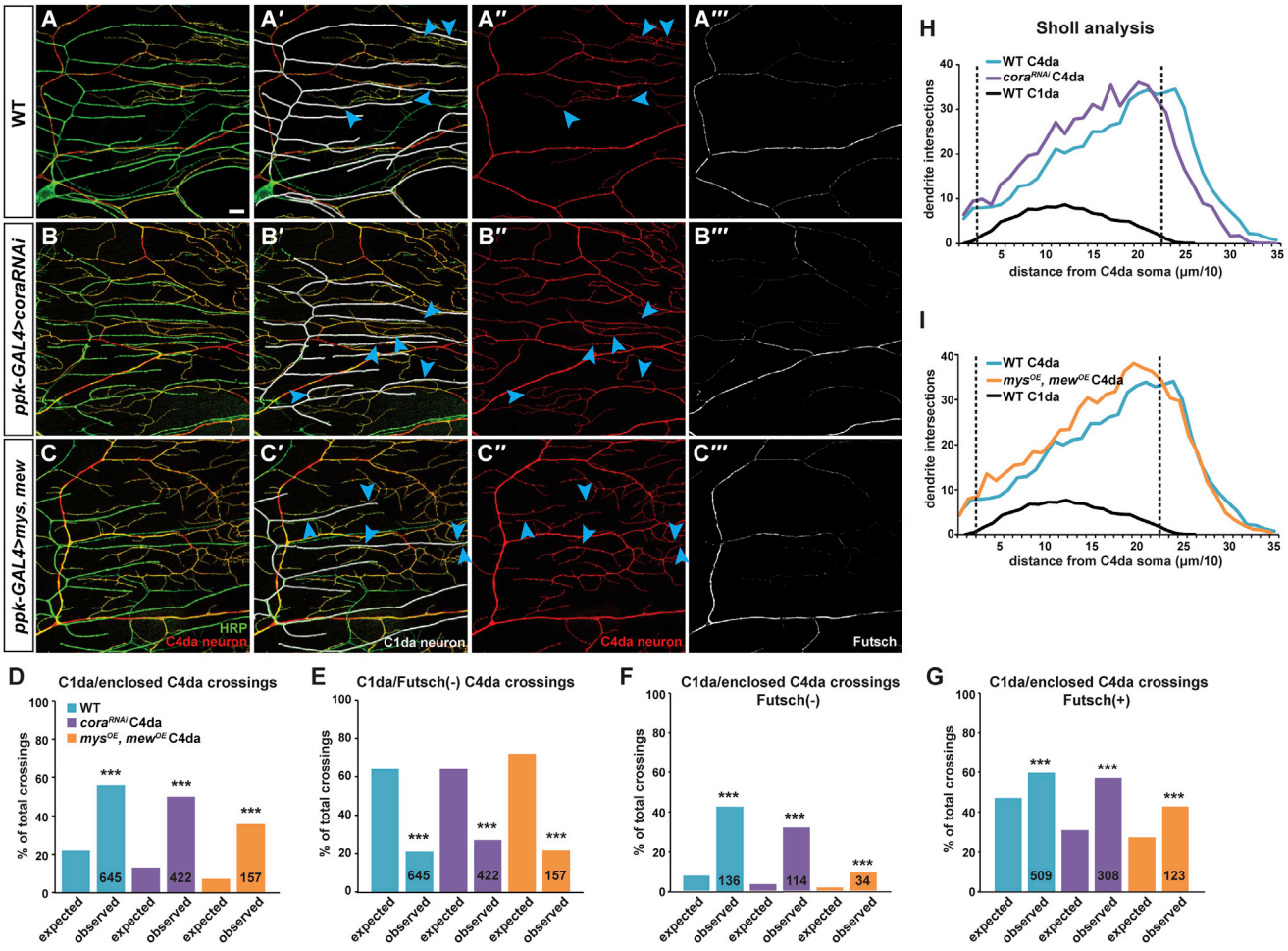

Figure 6. Dendrites of C4da and C1da Neurons Exhibit Heterotypic Avoidance

(A–C) Covisualization of C4da and C1da neurons sharing the same field. (A) WT C4da and C1da neurons. (B) C4da neurons expressing *UAS-coraRNAi*. (C) C4da neurons expressing *UAS-mys* and *UAS-mew*. *ppk-GAL4* was used to drive expression of transgenes and *UAS-CD4:tdTom* (red). The minimally enclosed C1da neurons (see Figure S6) and the non-enclosed segments of C4da neurons were detected by anti-HRP immunostaining (green). Stabilized microtubules were labeled with anti-Futsch antibody. (A–C) Merge of red and green channels. (A′–C′) C1da neurons in (A)–(C) are traced in white. (A″–C″) C4da neuron dendrites only (red channel). (A‴–C‴) Anti-Futsch immunofluorescence. Cyan arrows indicate intercalation between dendrites of C1da neurons and Futsch(−) dendrites of C4da neurons.

(D) Quantification of crossings between C1da dendrites and enclosed dendrites of WT, $cora^{RNAi}$, or *mys, mew*-overexpressing C4da neurons. Expected frequency of dendrite crossings was defined by the percentage of C4da dendrite length that is enclosed. Here and below, expected frequencies were compared to observed frequencies using a chi-square test, ***$p < 0.001$. The total number of observed crossings between C4da and C1da neuron pairs is indicated.

(E) Quantification of crossings between C1da dendrites and Futsch(−) C4da dendrites of WT, $cora^{RNAi}$, or *mys, mew*-overexpressing C4da neurons. Expected frequency of dendrite crossings was defined by the percentage of C4da dendrite length that is Futsch(−).

(F) Crossings between C1da neuron dendrites and enclosed, Futsch(−) C4da neuron dendrites. Expected frequency of dendrite crossings was defined by the percentage of C4da neuron dendrite length that is both enclosed and Futsch(−).

(G) Crossings between C1da neuron dendrites and enclosed, Futsch(+) C4da neuron dendrites. Expected frequency of dendrite crossings was defined by the percentage of C4da neuron dendrite length that is both enclosed and Futsch(+).

(H and I) Sholl analysis of C4da and C1da neurons, with respect to C4da neuron soma.

All images are confocal z series projections. Scale bar, 10 μm.

whether the maintenance of C1da neuron arbors depends on enclosure of C3da neurons, we analyzed the effect of decreasing enclosure of the C3 ddaF neuron on C1 ddaE and ddaD neurons. Dendrites of the anterior-facing ddaD neuron partially overlap dendrites of the ddaF neuron, whereas the ddaE neuron shares little, if any, of its field with the ddaF neuron (Figures S7A, S7A′, S7C, S7C′, and S7E). In contrast to C4da neurons, overexpression of *mys* and *mew* in C3da neurons did not affect ddaE neuron morphogenesis (Figures S7B, S7D, S7F, and S7G). However, *mys, mew* overexpression in C3da neurons did cause loss of small dendrites in ddaD, without affecting total dendrite length (Figures S7F and S7G). Together

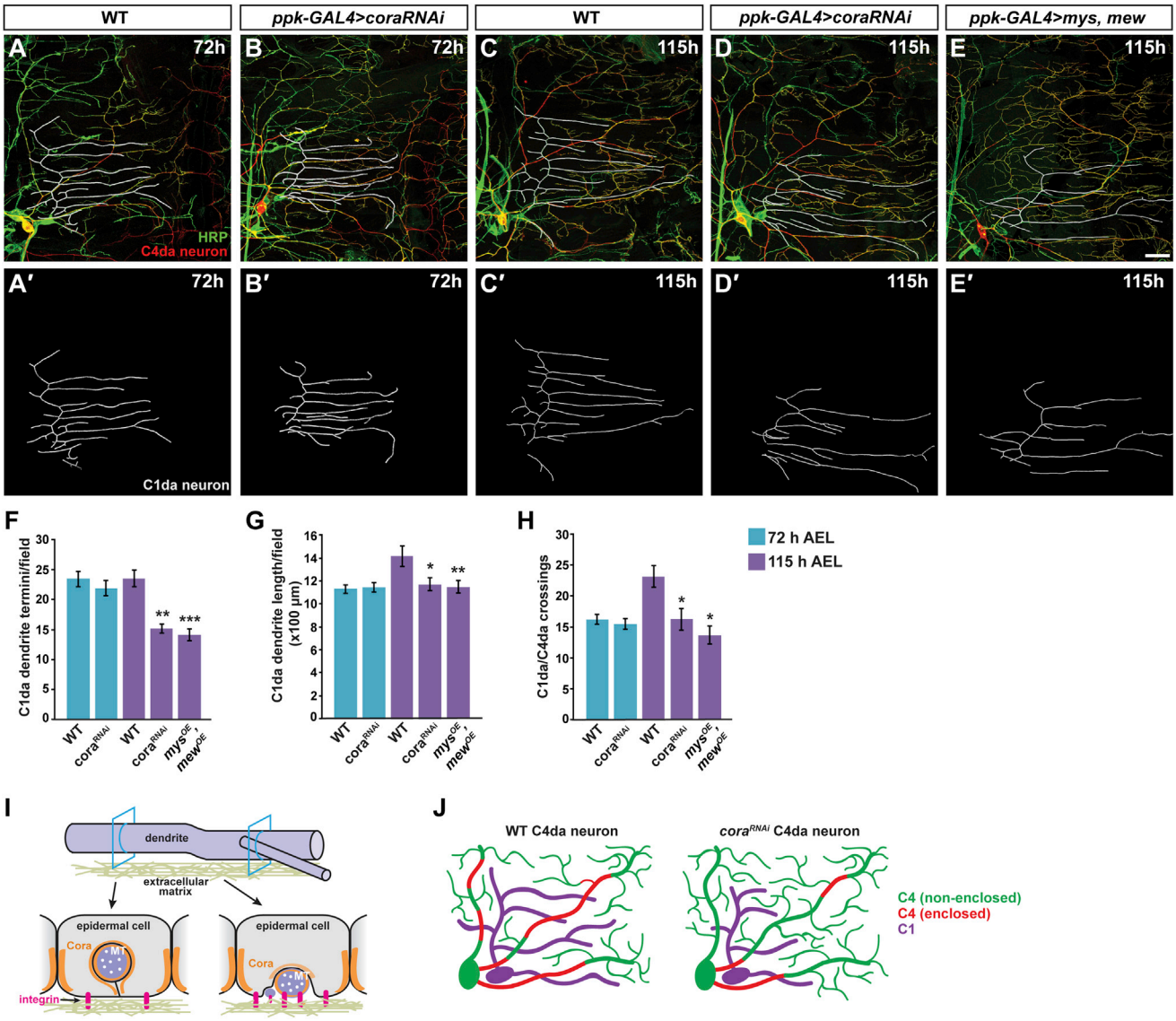

Figure 7. Enclosure of C4da Neurons Permits C1da Neuron Morphogenesis

(A–E) Covisualization of C4da and C1da neurons at 72 hr AEL (A and B) and 115 hr AEL (C–E). C4da neurons (red) were visualized using *ppk-GAL4, UAS-CD4:tdTom* (red). C1da neurons, as well as non-enclosed segments of C4da neurons, were detected by anti-HRP immunostaining before permeabilization (green). (A and C) WT neurons. (B and D) $cora^{RNAi}$ C4da neurons. (E) *mys, mew* overexpression in C4da neurons. (A′–E′) Tracings of C1da neurons in (A)–(E).

(F) Quantification of C1da neuron total dendrite length.

(G) Quantification of C1da neuron dendritic termini.

(H) Quantification of crossings between C4da neurons and C1da neurons.

(I and J) Model of Cora-mediated dendrite enclosure. (I) Cora is localized to the epidermal cell membrane and the dendrite membrane in C4da neurons. Adhesive interactions mediated by Cora facilitate dendrite enclosure by epidermal cells. Enclosure locally restricts branching. (J) Reduced enclosure of C4da neurons results in excess dendrite growth in proximal regions of the dendritic field. Reduced enclosure, coupled with excess dendrite growth, impedes development of C1da neurons.

All images are confocal z series projections. Scale bar, 30 μm. Values are mean ± SEM; *$p < 0.05$, **$p < 0.01$, ***$p < 0.001$, as assessed by Student's t test. See also Figure S7.

with our data showing C4da-C1da neuron dendrite interactions, these results indicate that the non-cell-autonomous requirement for C3da and C4da neuron enclosure in C1da neuron morphogenesis correlates with the degree of dendritic overlap between neuron pairs.

DISCUSSION

Dendrite morphogenesis depends on a complex interplay of intrinsic neuronal factors, systemic growth cues, interaction with growth substrates, and signals from neighboring neuronal

and non-neuronal cells (Dong et al., 2015). Studies presented here have uncovered a developmental program through enclosure of dendrites by epidermal cells that ensures coordination of growth among different classes of *Drosophila* da neurons that innervate a common territory.

Balancing Local Neuron-ECM Interactions to Regulate Growth

We show that dendrite enclosure by epidermal cells is facilitated by the membrane-associated protein Cora, which is required in both C4da neurons and in epidermal cells (Figure 7I). Cora-mediated enclosure locally restricts branching by both restricting dendrite growth and promoting dendrite retraction; it is unclear, however, whether enclosure restricts branching directly, through local regulation of the cytoskeleton, or indirectly, by limiting dendrite access to ECM-derived growth cues. Although less likely, self-avoidance of unenclosed dendrites could promote branching.

Adhesion of non-enclosed dendrites to the ECM via integrin-laminin interactions promotes dendrite maintenance (Kim et al., 2012). As Kim et al. (2012) have suggested, local differences in the strength of cell-cell adhesion versus cell-ECM adhesion are likely to play a role in determining which segments of da neuron dendrites become enclosed by epidermal cells and which segments are free to grow and branch. We find that Cora and integrins play functionally opposing roles in the regulation of dendrite enclosure and branching (Figure 7I). In epithelial cells, Cora localizes to septate junctions at the basolateral membrane, whereas integrins facilitate attachment of the basal membrane to the ECM. Cora and integrins may likewise occupy distinct membrane domains in da neurons, perhaps segregating along the dendritic apical-basal or proximal-distal axes. Future study of their subcellular localization in dendrites may thus provide insights into the mechanisms that govern where dendrite enclosure and branching occur.

Localized Epithelial-like Compartments within the Dendrite Arbor

Adhesion between sensory neurons and support cells is important in a number of developmental contexts, including patterning of *C. elegans* mechanosensory neurons and spacing of zebrafish photoreceptors (Dong et al., 2013; Salzberg et al., 2013; Zou et al., 2012). Our results point to roles for sensory neuron-support cell adhesion in permitting dendrite enclosure, locally restricting branching, and coordinating development of different sensory neuron types. While the precise nature of adhesion between C4da neurons and epidermal cells remains a focus for future investigation, the requirement for the epithelial septate junction components Cora and Nrx-IV in both neuronal and epidermal cell types and the close apposition of Cora protein in dendrites and enclosing epidermal cells raise the possibility that these proteins have been repurposed for use in a symmetrical neuro-epidermal adhesive junction. Whereas ATPα is also required in neurons, we do not find evidence of a similar requirement for Yrt, suggesting that some members of the Cora polarity and septate junction groups may function together only in a context-dependent manner.

Enclosure is more prevalent along large dendrites that harbor stabilized, organized microtubule populations. Although Cora facilitates enclosure independent of dendritic microtubule content, the presence of stabilized microtubules in dendrites might also promote enclosure, perhaps by facilitating trafficking of factors required for enclosure or by promoting dendrite stabilization. The idea that dendrite cytoskeletal organization may be an important factor for dendrite enclosure is supported by the observation that the actin-organizing Rho family guanosine triphosphatase (GTPase), Rac1, is required to restrict enclosure (Soba et al., 2015). Other factors, such as the size of the dendrite, may additionally play roles in mediating enclosure. Analogously, vertebrate axon myelination depends on axon fiber size, which is communicated to Schwann cells by axonal Neuregulin-1 (Michailov et al., 2004). If dendrite size plays a role in enclosure by epidermal cells, Cora, which appears to be enriched in large dendrites, could be one factor that communicates this information. Furthermore, local enrichment of Cora in these dendrites suggests that there are local epithelial-like dendrite compartments.

Coordinated Growth of Functionally Diverse Neurons within a Receptive Field

We find that enclosure of the morphologically complex da neurons ddaC and ddaF minimizes contact-dependent retraction of C1da neuron dendrites and maximizes dendritic field coverage among different types of da neurons (Figure 7J). Repulsion between C4da and C1da neuron dendrites occurs when both are engineered to express the same isoform of the Down syndrome cell adhesion molecule (DSCAM), suggesting that DSCAM diversity is a requirement for coexistence of different classes of da neurons that share the same territory (Soba et al., 2007). However, our observation that C1da and Futsch(−) C4da neuron dendrites normally exhibit heterotypic avoidance indicates that while DSCAM diversity may be permissive, it is not sufficient for heterotypic coexistence. We find that local dendritic compartments have differential capacities for coexistence with dendrites of other neurons, revealing a potential mechanism of neuronal organization. For *Drosophila* da neurons, enclosure appears to play an active role in coordinating spatial organization of overlapping neurons by separating heterotypic dendrites in 3D space and locally limiting the prevalence of dendrites that lack stable microtubules. The mechanism by which different dendritic compartments are able to adopt differential capacities for heterotypic interaction remains an intriguing avenue for future investigation. As in *Drosophila*, the vertebrate epidermis is innervated by multiple types of sensory neurons (Lumpkin and Caterina, 2007; Palanca et al., 2013), and it will be interesting to determine whether neuron-neuron and neuron-epidermal interactions that regulate dendrite morphogenesis in *Drosophila* similarly influence neurite morphogenesis and receptive field innervation in vertebrate sensory neurons. Similarly, it will be important to explore whether the principles for coordinated neuronal development we uncovered in *Drosophila* da neurons extend to other contexts of neuronal development, such as in the mammalian CNS.

EXPERIMENTAL PROCEDURES

Fly Stocks

The following reporters were used to visualize C4da neurons: *ppk-GAL4, UAS-CD4:tdTom*; *ppk-GAL4, UAS-CD4:tdGFP*; *GAL4^{477}, UAS-CD4:tdTom*;

GAL4^{477}, *UAS-CD4:td*GFP (Bhogal et al., 2016); *ppk-CD4:tdTom* and *ppk-CD4:tdGFP* (Han et al., 2011). C1da neurons were visualized using *GAL4*^{221}, *UAS-mCD8:GFP* (Grueber et al., 2003), and C3da neurons were visualized with *UAS-mCD8:GFP* and *GAL4*$^{1003.3}$ (Hughes et al., 2007). Epidermal expression was driven using *hh-GAL4* (Tanimoto et al., 2000). The *cora*^{14} (Lamb et al., 1998) and *cora*^{k08713} (Spradling et al., 1999) alleles were used. Data shown were obtained using RNAi lines from the Vienna *Drosophila* RNAi Center (VDRC) (*UAS-coraRNAi*^{108749}, *UAS-Nrx-IVRNAi*^{108128}, and *UAS-mysRNAi*^{103704}) and the Harvard Transgenic RNAi Project (TRiP)/Bloomington *Drosophila* Stock Center (BDSC) (*UAS-yrtRNAi*^{36118} and *UAS-Atp*α*RNAi*^{33646}). Phenotypes were confirmed using TRiP lines: *UAS-mysRNAi*^{33642}. *UAS-coraRNAi*^{28933}, *UAS-coraRNAi*^{35003}, and *UAS-Nrx-IVRNAi*^{2871}. We confirmed reduction of Yrt protein levels by expression of *UAS-yrtRNAi*^{36118} in ovarian follicle cells with *tj-GAL4* (data not shown). Efficacy of *UAS-Atp*α*RNAi*^{33646} has previously been demonstrated (Luan et al., 2014). Integrin overexpression was performed using *UAS-*α*PS1 (mew)* and *UAS-*β*PS (mys)*, provided by K. Broadie (Vanderbilt University). *UAS-myc-cora*$^{1-1698}$ (Ward et al., 2001) was a gift from R. Fehon (University of Chicago). Crosses were performed at 29°C to enhance GAL4/UAS efficiency.

Immunofluorescence

Immunofluorescence was performed as previously described (Bhogal et al., 2016; Grueber et al., 2002). Unless otherwise noted, wandering third instar larvae were selected for analysis. Body wall muscle was manually removed from filleted third instar larvae (Tenenbaum and Gavis, 2016), except for experiments assaying the number of dendritic terminal branches. Larvae were fixed in 4% paraformaldehyde in PBS for 25 min at room temperature (RT) and then washed with PBS. After permeabilization in PBS/0.3% Triton X-100 (PBT-X), larval fillets were incubated with Image-iT (Thermo Fisher Scientific) for 30 min, blocked for 1 hr in PBT-X/5% normal goat serum (NGS), and incubated with primary antibody diluted in PBT-X/5% NGS. Labeling with anti-HRP in the absence of Triton X-100 was performed as previously described (Kim et al., 2012), with the following modifications: samples were incubated with Alexa Fluor-conjugated goat anti-HRP (Jackson ImmunoResearch, 123-545-021 and 123-585-021, 1:200) for 1 hr at room temperature in PBS/5% NGS and washed 3 × 15 min in PBS before proceeding to subsequent steps, as outlined earlier. Primary antibodies were obtained from the Developmental Studies Hybridoma Bank (DSHB) at the University of Iowa: anti-Coracle (C615.16, 1:20), anti-Mys (CF.6G11, 1:20), anti-Dlg (4F3, 1:10), and anti-Futsch (22C10, 1:20). Neuronal morphology was visualized with Alexa Fluor 488 rabbit anti-GFP (Life Technologies, A21311, 1:350), mouse anti-GFP (Abcam, Ab1218, 1:500), or rabbit anti-dsRed (Clontech, 632496, 1:1,000) depending on the membrane marker. Species and isotype-specific secondary antibodies were obtained from Life Technologies: Alexa Fluor 488 goat anti-mouse immunoglobulin G1 (IgG1) (A21121, 1:1,000), Alexa Fluor 568 goat anti-rabbit (A11011, 1:1,000), Alexa Fluor 633 goat anti-mouse IgG1 (A21126, 1:500), and Alexa Fluor 633 immunoglobulin G2b (IgG2b) (A21146, 1:500). Double-labeling for Cora and Mys was performed sequentially with samples labeled first with anti-Cora and Alexa Fluor 488 goat anti-mouse IgG1 and then with anti-Mys and Alexa Fluor 633 goat anti-mouse IgG2b. All samples were mounted in Vectashield (Vector Labs).

Microscopy

Confocal imaging was performed using a Leica SPE microscope with 20×/0.7 numerical aperture (NA) air objective or 40×/1.25 NA oil objective. DdaC, ddaE, ddaF, and ddaD neurons in larval segments A3–A5 were imaged. Somas were placed in a similar location within the field of view for all samples in an experiment. For time-lapse analysis, larvae were imaged live at 72 hr AEL (with the specific neuron and segment noted) and then returned to food and housed individually until 115 hr AEL, at which point the specific neuron or segment previously noted was re-imaged. Neuron-specific Cora was imaged using a Zeiss LSM 800 microscope with AiryScan and 63×/1.4 NA oil objective. SIM was performed using a GE DeltaVision OMX microscope with 60×/1.42 NA oil objective. For live imaging of individual neurons, larvae aged 72 hr AEL were mounted individually in a 1:1 mix of Halocarbon 95 and Halocarbon 200 oil and imaged on a Leica SPE confocal microscope using a 40×/1.25 NA oil objective. Larvae were removed from the oil and aged in isolation on *Drosophila* media. At 115 hr AEL, larvae were mounted in a 1:2:2 mix of chloroform, Halocarbon 95, and Halocarbon 200 for re-imaging.

Quantitative Analyses

For all experiments, at least 10 neurons and 5 animals were imaged and analyzed for each genotype. Time-lapse images and the number of dendritic termini per image field were quantified from z series projections using ImageJ software. "Retracting dendrites" were defined as dendrites that disappeared or whose length decreased from 72 to 115 hr AEL. "Growing dendrites" were defined as new dendrites or dendrites whose length increased from 72 to 115 hr AEL. Automated Sholl analysis was performed on z series projections in ImageJ using the Sholl_Analysis plugin (Ferreira et al., 2014). Sholl analyses of ddaE neurons and the dorsal-posterior quadrant of ddaC neurons were performed with respect to the ddaC neuron soma. Dendrite lengths (total length, enclosed length, and Futsch(+) length) and branch densities were quantified using Imaris 7.6.4 software (Bitplane, Zurich, Switzerland). Dendrites were traced manually using the filaments function. Enclosure, Futsch(+) length, and branch density of ddaC neurons were quantified blindly. Only the dorsal-posterior quadrants of ddaC neurons were analyzed, and dendrites innervating segment boundaries were omitted from analysis. Enclosed segments were identified by a low HRP signal, and non-enclosed segments were identified by a high HRP signal or by the presence or absence of Dlg enrichment. For clarity, colors in some images were inverted in Imaris. In addition, Futsch labeling was masked using the Imaris surfaces function to show only ddaC-colocalized Futsch. Bar graphs show mean ± SEM; p values are indicated by *$p < 0.05$, **$p < 0.01$, and ***$p < 0.001$, as assessed by Student's t test. Observed frequencies of crossing events between ddaC and ddaE neurons were compared to expected frequencies using a chi-square test (***$p < 0.001$). Expected frequencies were defined using the percentage (by length) of ddaC dendrite type present in the ddaC dorsal-posterior quadrant.

SUPPLEMENTAL INFORMATION

Supplemental Information includes seven figures and can be found with this article online at http://dx.doi.org/10.1016/j.celrep.2017.09.001.

AUTHOR CONTRIBUTIONS

Conceptualization, C.M.T., M.M., and E.R.G.; Methodology, C.M.T. and M.M.; Investigation, C.M.T., M.M., and R.A.A.; Formal Analysis, C.M.T., M.M., and R.A.A.; Writing, C.M.T., M.M., and E.R.G.; Funding Acquisition, E.R.G.

ACKNOWLEDGMENTS

We thank K. Broadie, R. Fehon, Y.N. Jan, the BDSC, the TRiP, and the VDRC for fly stocks; the DSHB for antibodies; and G. Laevsky for assistance with microscopy. We also thank W. Grueber for helpful discussions and B. Bhogal, E. Olesnicky, and J. Tamayo for comments on the manuscript. C.M.T. and R.A.A. were supported by NIH training grant T32 GM007388. This work was supported by NIH grants R01 GM067758 and R01 GM061107 to E.R.G.

Received: December 11, 2016
Revised: August 24, 2017
Accepted: August 31, 2017
Published: September 26, 2017

REFERENCES

Baines, A.J., Lu, H.C., and Bennett, P.M. (2014). The Protein 4.1 family: hub proteins in animals for organizing membrane proteins. Biochim. Biophys. Acta *1838*, 605–619.

Bhogal, B., Plaza-Jennings, A., and Gavis, E.R. (2016). Nanos-mediated repression of *hid* protects larval sensory neurons after a global switch in sensitivity to apoptotic signals. Development *143*, 2147–2159.

Dong, X., Liu, O.W., Howell, A.S., and Shen, K. (2013). An extracellular adhesion molecule complex patterns dendritic branching and morphogenesis. Cell *155*, 296–307.

Dong, X., Shen, K., and Bülow, H.E. (2015). Intrinsic and extrinsic mechanisms of dendritic morphogenesis. Annu. Rev. Physiol. *77*, 271–300.

Fehon, R.G., Dawson, I.A., and Artavanis-Tsakonas, S. (1994). A *Drosophila* homologue of membrane-skeleton protein 4.1 is associated with septate junctions and is encoded by the *coracle* gene. Development *120*, 545–557.

Ferreira, T., Ou, Y., Li, S., Giniger, E., and van Meyel, D.J. (2014). Dendrite architecture organized by transcriptional control of the F-actin nucleator Spire. Development *141*, 650–660.

Grueber, W.B., Jan, L.Y., and Jan, Y.N. (2002). Tiling of the *Drosophila* epidermis by multidendritic sensory neurons. Development *129*, 2867–2878.

Grueber, W.B., Ye, B., Moore, A.W., Jan, L.Y., and Jan, Y.N. (2003). Dendrites of distinct classes of *Drosophila* sensory neurons show different capacities for homotypic repulsion. Curr. Biol. *13*, 618–626.

Hamdan, F.F., Gauthier, J., Araki, Y., Lin, D.T., Yoshizawa, Y., Higashi, K., Park, A.R., Spiegelman, D., Dobrzeniecka, S., Piton, A., et al.; S2D Group (2011). Excess of de novo deleterious mutations in genes associated with glutamatergic systems in nonsyndromic intellectual disability. Am. J. Hum. Genet. *88*, 306–316.

Han, C., Jan, L.Y., and Jan, Y.N. (2011). Enhancer-driven membrane markers for analysis of nonautonomous mechanisms reveal neuron-glia interactions in *Drosophila*. Proc. Natl. Acad. Sci. USA *108*, 9673–9678.

Han, C., Wang, D., Soba, P., Zhu, S., Lin, X., Jan, L.Y., and Jan, Y.N. (2012). Integrins regulate repulsion-mediated dendritic patterning of *Drosophila* sensory neurons by restricting dendrites in a 2D space. Neuron *73*, 64–78.

Hattori, Y., Usui, T., Satoh, D., Moriyama, S., Shimono, K., Itoh, T., Shirahige, K., and Uemura, T. (2013). Sensory-neuron subtype-specific transcriptional programs controlling dendrite morphogenesis: genome-wide analysis of Abrupt and Knot/Collier. Dev. Cell *27*, 530–544.

Hughes, M.E., Bortnick, R., Tsubouchi, A., Bäumer, P., Kondo, M., Uemura, T., and Schmucker, D. (2007). Homophilic Dscam interactions control complex dendrite morphogenesis. Neuron *54*, 417–427.

Jiang, N., Soba, P., Parker, E., Kim, C.C., and Parrish, J.Z. (2014). The microRNA *bantam* regulates a developmental transition in epithelial cells that restricts sensory dendrite growth. Development *141*, 2657–2668.

Jung, Y., and McCarty, J.H. (2012). Band 4.1 proteins regulate integrin-dependent cell spreading. Biochem. Biophys. Res. Commun. *426*, 578–584.

Kim, M.E., Shrestha, B.R., Blazeski, R., Mason, C.A., and Grueber, W.B. (2012). Integrins establish dendrite-substrate relationships that promote dendritic self-avoidance and patterning in *Drosophila* sensory neurons. Neuron *73*, 79–91.

Lamb, R.S., Ward, R.E., Schweizer, L., and Fehon, R.G. (1998). *Drosophila coracle*, a member of the protein 4.1 superfamily, has essential structural functions in the septate junctions and developmental functions in embryonic and adult epithelial cells. Mol. Biol. Cell *9*, 3505–3519.

Laprise, P., Lau, K.M., Harris, K.P., Silva-Gagliardi, N.F., Paul, S.M., Beronja, S., Beitel, G.J., McGlade, C.J., and Tepass, U. (2009). Yurt, Coracle, Neurexin IV and the Na(+),K(+)-ATPase form a novel group of epithelial polarity proteins. Nature *459*, 1141–1145.

Luan, Z., Reddig, K., and Li, H.S. (2014). Loss of Na(+)/K(+)-ATPase in *Drosophila* photoreceptors leads to blindness and age-dependent neurodegeneration. Exp. Neurol. *261*, 791–801.

Lumpkin, E.A., and Caterina, M.J. (2007). Mechanisms of sensory transduction in the skin. Nature *445*, 858–865.

MacKrell, A.J., Blumberg, B., Haynes, S.R., and Fessler, J.H. (1988). The *lethal myospheroid* gene of *Drosophila* encodes a membrane protein homologous to vertebrate integrin beta subunits. Proc. Natl. Acad. Sci. USA *85*, 2633–2637.

McLachlan, I.G., and Heiman, M.G. (2013). Shaping dendrites with machinery borrowed from epithelia. Curr. Opin. Neurobiol. *23*, 1005–1010.

Michailov, G.V., Sereda, M.W., Brinkmann, B.G., Fischer, T.M., Haug, B., Birchmeier, C., Role, L., Lai, C., Schwab, M.H., and Nave, K.A. (2004). Axonal neuregulin-1 regulates myelin sheath thickness. Science *304*, 700–703.

Misra, M., Edmund, H., Ennis, D., Schlueter, M.A., Marot, J.E., Tambasco, J., Barlow, I., Sigurbjornsdottir, S., Mathew, R., Vallés, A.M., et al. (2016). A genome-wide screen for dendritically localized RNAs identifies genes required for dendrite morphogenesis. G3 (Bethesda) *6*, 2397–2405.

O'Brien, G.S., Rieger, S., Wang, F., Smolen, G.A., Gonzalez, R.E., Buchanan, J., and Sagasti, A. (2012). Coordinate development of skin cells and cutaneous sensory axons in zebrafish. J. Comp. Neurol. *520*, 816–831.

Palanca, A.M., Lee, S.L., Yee, L.E., Joe-Wong, C., Trinh, L.A., Hiroyasu, E., Husain, M., Fraser, S.E., Pellegrini, M., and Sagasti, A. (2013). New transgenic reporters identify somatosensory neuron subtypes in larval zebrafish. Dev. Neurobiol. *73*, 152–167.

Roos, J., Hummel, T., Ng, N., Klämbt, C., and Davis, G.W. (2000). *Drosophila* Futsch regulates synaptic microtubule organization and is necessary for synaptic growth. Neuron *26*, 371–382.

Salzberg, Y., Díaz-Balzac, C.A., Ramirez-Suarez, N.J., Attreed, M., Tecle, E., Desbois, M., Kaprielian, Z., and Bülow, H.E. (2013). Skin-derived cues control arborization of sensory dendrites in *Caenorhabditis elegans*. Cell *155*, 308–320.

Soba, P., Zhu, S., Emoto, K., Younger, S., Yang, S.J., Yu, H.H., Lee, T., Jan, L.Y., and Jan, Y.N. (2007). *Drosophila* sensory neurons require Dscam for dendritic self-avoidance and proper dendritic field organization. Neuron *54*, 403–416.

Soba, P., Han, C., Zheng, Y., Perea, D., Miguel-Aliaga, I., Jan, L.Y., and Jan, Y.N. (2015). The Ret receptor regulates sensory neuron dendrite growth and integrin mediated adhesion. eLife *4*, e05491.

Spradling, A.C., Stern, D., Beaton, A., Rhem, E.J., Laverty, T., Mozden, N., Misra, S., and Rubin, G.M. (1999). The Berkeley *Drosophila* Genome Project gene disruption project: single P-element insertions mutating 25% of vital *Drosophila* genes. Genetics *153*, 135–177.

Stewart, A., Tsubouchi, A., Rolls, M.M., Tracey, W.D., and Sherwood, N.T. (2012). Katanin p60-like1 promotes microtubule growth and terminal dendrite stability in the larval class IV sensory neurons of *Drosophila*. J. Neurosci. *32*, 11631–11642.

Tanimoto, H., Itoh, S., ten Dijke, P., and Tabata, T. (2000). Hedgehog creates a gradient of DPP activity in *Drosophila* wing imaginal discs. Mol. Cell *5*, 59–71.

Tenenbaum, C.M., and Gavis, E.R. (2016). Removal of *Drosophila* muscle tissue from larval fillets for immunofluorescence analysis of sensory neurons and epidermal cells. J. Vis. Exp. *117*, e54670.

Ward, R.E., 4th, Lamb, R.S., and Fehon, R.G. (1998). A conserved functional domain of *Drosophila* coracle is required for localization at the septate junction and has membrane-organizing activity. J. Cell Biol. *140*, 1463–1473.

Ward, R.E., 4th, Schweizer, L., Lamb, R.S., and Fehon, R.G. (2001). The protein 4.1, ezrin, radixin, moesin (FERM) domain of *Drosophila* Coracle, a cytoplasmic component of the septate junction, provides functions essential for embryonic development and imaginal cell proliferation. Genetics *159*, 219–228.

Yee, G.H., and Hynes, R.O. (1993). A novel, tissue-specific integrin subunit, beta nu, expressed in the midgut of *Drosophila melanogaster*. Development *118*, 845–858.

Zhang, H., Wang, Y., Wong, J.J., Lim, K.L., Liou, Y.C., Wang, H., and Yu, F. (2014). Endocytic pathways downregulate the L1-type cell adhesion molecule neuroglian to promote dendrite pruning in *Drosophila*. Dev. Cell *30*, 463–478.

Zou, J., Wang, X., and Wei, X. (2012). Crb apical polarity proteins maintain zebrafish retinal cone mosaics via intercellular binding of their extracellular domains. Dev. Cell *22*, 1261–1274.